International Journal of Biological Macromolecules 213 (2022) 1018–1028

Contents lists available at ScienceDirect

International Journal of Biological Macromolecules

journal homepage: www.elsevier.com/locate/ijbiomac

Cupric oxide nanoparticles incorporated poly(hydroxybutyrate) nanocomposite for potential biosensing application

Muhammad Junaid Bakhtiyar [a], Zulfiqar Ali Raza [a,*], Muhammad Aslam [a,*], Sadia Zafar Bajwa [b], Muhammad Shoaib ur Rehman [a], Samvia Rafiq [a]

[a] Department of Applied Sciences, National Textile University, Faisalabad 37610, Pakistan
[b] National Institute for Biotechnology and Genetic Engineering, Faisalabad 577, Pakistan

ARTICLE INFO

Keywords:
Biosensing
Nanobiocomposite
Polyhydroxybutyrate

ABSTRACT

We report the synthesis of a novel electrochemical biosensor comprising of cupric oxide (CuO) nanoparticles (NPs) mediated poly(hydroxybutyrate) (PHB) composite film with polyvinyl alcohol (PVA) as a binder/template support using the solution casting method for the detection of a biomolecule i.e., ascorbic acid (AA). The specimens were characterized for surface, chemical, mechanical, optical, and electrochemical attributes. The results expressed regular mediation of CuO NPs in the PHB/PVA matrix towards nanobiocomposite formation with enhanced crystallinity, inter-molecular interactions, mechanical, and electrochemical attributes, and decreased hydrophilicity and bandgap, thus being useful in potential optoelectronic devices. The synthesized biocomposite film exhibited a tensile strength of 86.24 ± 4.10 N which might be due to reinforcement/uniform dispersion of the CuO nanofiller in the PHB-based matrix. The PHB/CuO composite, then, deposited on a glassy carbon electrode surface exhibited good electrocatalytic activity towards the AA in the aqueous media even at low analyte concentrations. Such modified electrode surfaces with metal/biopolymer complex could find possible applications in the detection of other bioactive molecules.

1. Introduction

Sensors are the integrated analytical devices employed based on specific mechanisms to recognize or determine an analyte or a physical property and respond, accordingly [1]; examples are gas, pressure, bio-, and chemical sensors [2]. They are employed in widespread applications such as in food to detect any toxins, fire industry to detect any hazardous gases, and in controlling armours and executing biomedical diagnostics [3,4]. Generally, biosensors are either comprised of any biomaterial or used to recognize any biomolecule for life science applications such as in molecular biology, diagnostics, bio-telemedicine, food safety control, drug discovery, environmental biology, and so on [5,6]. An electrochemical biosensor usually comprises a set of electrodes that may translate a redox change into an electrical signal in terms of current density, conductance, resistance, or capacitance against an applied electrical potential on the biosensor's surface. Such devices possess a biological recognition system comprising some bioactive species such as nucleic acid, enzymes, cells, proteins, receptors, or antibodies that may interact specifically with the targeted analytes producing an electrical signal associated with the concentration of the test analyte [7]. The biosensors may be electrochemical, thermometric, optical, or piezoelectric based on working modes [1,8,9].

Synthetic polymers like polyethylene terephthalate, polyurethanes, polyacrylonitrile, etc. could be used as base-matrix for sensing applications due to their stability, flexibility, low weight, cost, disposability, and so on [10–12]. However, synthetic polymers are usually non-biodegradable and pose a serious threat to the environment. In the above context, poly(hydroxybutyrate) (PHB) might be evaluated as a sustainable alternative to synthetic polymers given its biodegradable, eco-friendly, and modifiable nature. However, it exhibits some inherent limitations for its widespread applications including high crystallinity and brittleness, low tensile strength, elongation, electrical conductivity, and large bandgap. Likewise, it may express poor selectivity and sensitivity for the said purposes. This limits its applications in electrochemical systems for biosensing applications [13]. This could be compensated by fabricating its composites with either intrinsic conducting polymers, nanocarbons [14], or some metal sulfides [15] and oxides [16,17]. The incorporation of conducting nanofillers might

* Corresponding authors.
E-mail addresses: zarazapk@yahoo.com (Z.A. Raza), aslamfaridipk@gmail.com (M. Aslam).

https://doi.org/10.1016/j.ijbiomac.2022.06.018
Received 27 March 2022; Received in revised form 20 May 2022; Accepted 5 June 2022
Available online 9 June 2022

enhance the structural, optical, and electrical properties of the resultant nanobiocomposites.

Cupric oxide (CuO) is a semi-conducting material with a monoclinic structure, which exhibits a direct bandgap of 2 eV. Its incorporation in polymer-based sensors may accelerate and sensitize the response owing to their significantly large surface area and porous structure. The CuO nanoparticles (NPs) incorporated in the polymer matrix may be a viable solution to address the drawbacks associated with polymer-based biosensors. The incorporation of CuO NPs into the PHB matrix may enhance the mechanical properties and impart electrical conductivity in the resultant nanocomposite desirable for electrochemical sensing devices. Such nanocomposites have received great attention for their potential applications in biosensing [18,19].

The biosensors reported in the literature express low stability and less reusability with weak sensitivity and delayed response which needs improvement in the electrochemical context. The present research

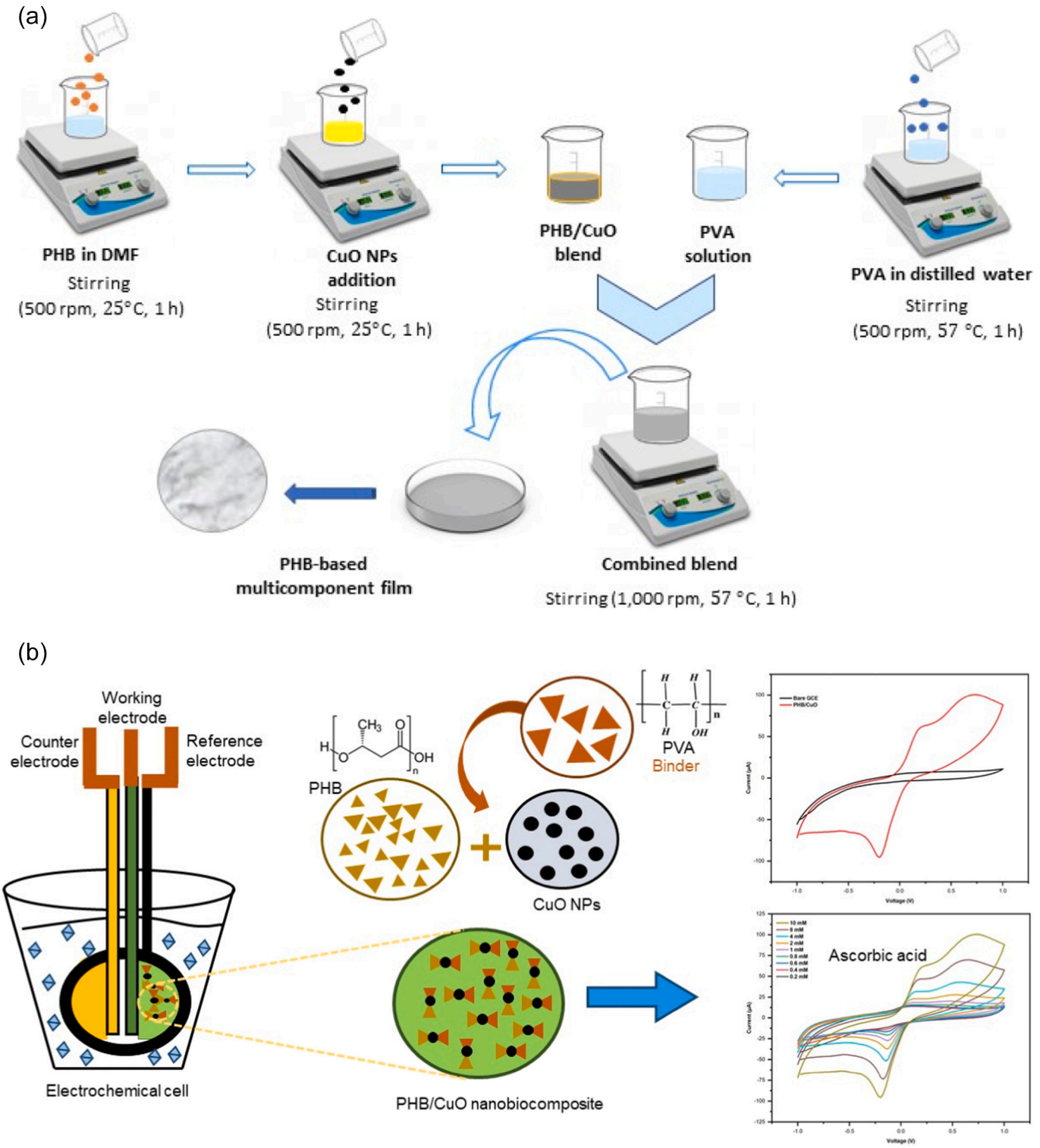

Fig. 1. Schematic illustrations of a) the synthesis of PHB-based nanobiocomposite film and b) over view of the study.

focuses on the fabrication of a metal-to-biopolymer complex for enhanced sensitivity and stability of biosensors comprised of CuO NPs mediated into the PHB matrix. The prepared PHB/CuO/PVA (designated nanobiocomposite) films were investigated using advanced analytical tools. The nanobiocomposite film was also deposited on a glassy carbon electrode (GCE) surface for electrochemical analysis. We found no report on the biosensing behavior of CuO NPs mediated by PHB nanobiocomposite films for electrochemical sensing of ascorbic acid (AA) in the aqueous media.

2. Materials and methods

2.1. Materials

Poly(hydroxybutyrate) (PHB), (molar mass = 362.5 g/mol), polyvinyl alcohol (PVA) $(C_2H_4O)_n$ M_W ~1500 g/mol, cupric oxide (CuO), dimethylformamide [DMF, $(CH_3)_2NCH$], potassium chloride (KCl), potassium ferricyanide (KFeCN), nitric acid, Nafion soution, ascorbic acid, phosphate-buffered saline (PBS, pH 7), *n*-hexane, *n*-hexadecane, toluene, and ethylene glycol were purchased from Sigma-Aldrich. All the materials were of analytical grade and used without any additional refinement processes.

2.2. Fabrication of nanobiocomposite films

The PHB-based nanobiocomposite films were prepared using the solution casting approach [20,21]. Briefly, PHB powder (3 %, *w*/w) was dispersed in DMF media under magnetic stirring at 500 rpm and 57 °C for 1 h. CuO NPs (1–3 %, *w*/w) were added to the prepared PHB solution and continued stirring for 1 h more. PVA (as 3 %, w/w) was separately dissolved in water via magnetic stirring under the same conditions. Both liquors were combined and homogenized at 1000 rpm and 57 °C for 1 h. The resultant mix was ultra-probe sonicated for 30 min to avoid any agglomeration in the blend and then transferred to a Petri plate and left to dry to constant mass in a vacuum oven at 40 °C. The dried nanobiocomposite film was peeled off and analyzed, accordingly. The schematic diagram illustrating the above process and overview of the study are shown in Fig. 1.

2.3. Analytical characterization

A scanning electron microscope (SEM) (FEI Quanta 250, USA) coupled with an energy-dispersive x-ray (EDX) and transmission electron detectors was used to examine the surface morphology and elemental analysis of the prepared samples, operated at an acceleration voltage of 15 kV. Attenuated total reflectance - Fourier transform infrared (ATR-FTIR) spectroscope (Bruker Tensor 27) operated in the wavenumber range of 4000–600 cm^{-1} was used to determine any chemical interactions among the precursors during nanocomposite formation. The crystalline patterns, properties, and phase purity of the prepared samples were assessed using an x-ray diffractometer (XRD, X'Pert XRD) containing a radiation source of CuKα (1.54 Å) operated in the 2θ range of 10–50°.

An optical tensiometer (Theta Lite) was employed to measure the water contact angle (WCA) of the prepared films at different time intervals. The surface energy profiles of the test films were measured using Young's Eq. (1):

$$\sigma_S = \sigma_{SL} + \sigma_L cos\theta \tag{1}$$

where, σ_S = surface energy of solid surface; σ_L = surface tension of liquid; σ_{SL} = interfacial tension between solid surface and liquid and θ = contact angle between solid and liquid. The Good's Eq. (2) expresses:

$$\sigma_{SL} = \sigma_S + \sigma_L - 2\left(\sigma_L^D \sigma_s^D\right)^{1/2} - 2\left(\sigma_L^P \sigma_s^P\right)^{1/2} \tag{2}$$

where, σ_L^D = dispersive component of liquid surface tension; σ_L^P = polar component of liquid surface tension; σ_S^D = dispersive component of solid surface energy and σ_S^P = polar component of solid surface energy. Combining Eqs. (1) and (2) implies that:

$$\frac{\sigma_{L\ (Cos\theta+1)}}{2\left(\sigma_L^D\right)^{1/2}} = \left(\sigma_s^P\right)^{1/2} \frac{\left(\sigma_L^P\right)^{1/2}}{\left(\sigma_L^D\right)^{1/2}} + \left(\sigma_s^D\right)^{1/2} \tag{3}$$

This is the equation of a straight line i.e., $y = mx + c$.

The tensile strength and elongation at the break of the specimens were recorded under the standard test method of ASTM D3822 using a universal testing machine (UTM, Instron 4302, USA). The absorption spectrums were acquired using a UV vis. spectrophotometer (UV-2800 BMS) in the 200–800 nm range. A frequency response analyzer (FRA, SA/RA-40 Core technology group, USA) was employed for the measurement of AC conductivity of the test specimens in the frequency range of 1 Hz to 8 MHz.

2.4. Fabrication of nanobiocomposite sensor

The sensors were prepared using the GCE polished with alumina slurries (average particle size 1.0, 0.3, and 0.05 μm) followed by washing in steps with ethanol, 1 M nitric acid, and deionized water, and finally purged under nitrogen. The cleaned mirrored electrode surface was drop-coated with 10 μL of CuO NPs-mediated PHB dispersion in water (as 9 μg/μL). The deposited layer was covered with a 0.2 μL drop of Nafion (10 %) and dried at room temperature. The hence prepared nanobiocomposite deposited GCE was used as a working electrode in the electrochemical analysis. In control experiments, the bare GCE was used, accordingly.

2.5. Electrochemical analysis

The cyclic voltammograms (CVs) were recorded using a potentiostat/galvanostat (Autolab) coupled with a three-electrodes system that includes modified GCE as the working electrode, Ag/AgCl as a reference electrode, and the glossy carbon rod as a counter electrode. The preliminary analyses were performed against the standard analyte of KFeCN (5 mM) in the presence of 1 M KCl as a supporting electrolyte in the aqueous media. Then, the electrochemical run was executed on PHB/CuO deposited GCE against AA in the PBS media (pH 7). Prior, all the solutions were purged with pure (99.99 %) nitrogen gas for the removal of any entrapped air bubbles. The C*V* analyses were carried out at different scan rates of 10, 50, and 100 mV s^{-1} in the potential range of −1.0 and 1.0 V at 25 °C. The environmental stability of the prepared sensor towards electrochemical sensing was evaluated by recording its CV response against the AA (10 mM) for up to three months at the scan rate of 100 mV s^{-1}. For that purpose, the nanobiocomposite deposited GCE surfaces were prior exposed to ambient conditions i.e., 25 °C with 65 % relative humidity.

3. Results and discussion

3.1. Synthesis chemistry of nanobiocomposite

It has been well established that inorganic nanofillers like CuO NPs significantly enhance the mechanical and electrical properties of polymer-based nanocomposites. The phenomena could be attributed to the structural re-orientation of constituent moieties towards uniform nano-dispersed composite film formation. The process, herein, could be controlled by H-bonding offered by the PVA matrix used both stabilizing as well as binding agent. The amphiphilic nature of PHB may allow polar interactions with the hydrophilic moieties both at PVA and CuO NPs where their hydrophobic segments develop dispersive interactions with the hydrocarbon chains. The large surface and crystalline nature of CuO NPs could allow the orientation of polymer segments over them in the

presence of PVA as the binder (Fig. 2). The physicochemical and electrical properties of the prepared samples have been described below.

3.2. Surface morphology

The SEM image of PHB/PVA blended film expressed a smooth surface and good miscibility of the precursors (Fig. 3a). The native CuO NPs exhibited spherical morphologies as expressed by the SEM/TEM images (Fig. 3b). The SEM images of nanobiocomposite expressed uniformity and regular mediation of CuO NPs in the PHB matrix (Fig. 3c) which might be facilitated by the H-bonding across the multi-components with PVA acting as the binding template [22]. The elemental analysis results of the test films have been placed on the corresponding SEM images. The results demonstrated that the PHB/PVA blended film expressed carbon (C) and oxygen (O) contents of 73.23 and 26.77 (%, *w*/w). The CuO NPs contained C and O contents as 85.22 and 14.78 (%, w/w), respectively; whereas on mediating them into the PHB/PVA matrix, the respective contents were revised to 54.69 and 13.21 (%, w/w), respectively, with the inclusion of copper (Cu) as 32.23 (%, w/w). The results demonstrated that oxygen-containing moieties in the nanocomposite films were reduced/less available due to their engagement with the CuO NPs under H-bonding thus making the resultant nanobiocomposite film less hydrophilic as is evident from WCA analysis [13].

3.3. FTIR analysis

The FTIR spectra of PVA, PHB, CuO NPs, and nanobiocomposite are shown in Fig. 4A. The characteristics transmission peaks for PVA were observed at 3290, 2920, 1708, 1430, 1370, 1245, 1084, and 840 cm^{-1} which were assigned to the hydroxy (O—H), -CH_2, carbonyl (C=O) stretching vibrations, C—H bending vibration of CH_2, C—H vibrational bands, C—H wagging, C—O stretching of acetyl groups and the C—C stretching vibration, respectively [23,24]. The native PHB expressed some weak peaks at 3443 cm^{-1} for the terminal -OH group, 2937 and 2969 cm^{-1} for the -CH_3 group, and 1452 cm^{-1} for the asymmetric bending of the -CH_2 (or -CH_3). The presence of an ester carbonyl group was indicated by a sharp peak at 1727 cm^{-1}, while those at 1282 cm^{-1} corresponded to the -CH stretching vibration and 1377 cm^{-1} to the asymmetric bending -CH_3 group of the PHB matrix [25]. The FTIR spectrum of CuO NPs showed a single peak at 1442 cm^{-1} which resembled the C—H stretching vibration [26]. The aforementioned precursors with some unavoidable peak shifts indicated their successful intercalation towards uniform nanobiocomposite formation. The peak associated with the -OH stretching vibration blue-shifted from 3290 to 3367 cm^{-1} which could be inferred to the H-bonding across the polar moieties at CuO NPs and the -OH prevailed on the polymer backbone [27]. The peak associated with carbonyl stretching blue-shifted from 1727 to 1720 cm^{-1} - which might be indicating enhanced carbonyl density both due to PVA and PHB matrices in the nanobiocomposite.

3.4. XRD analysis

The XRD patterns of PVA, PHB, CuO NPs, and nanobiocomposite are shown in Fig. 4B. A broad diffraction peak (1 0 1) at 2θ of 19.9° was observed indicating the semi-crystalline nature of the PVA matrix with an interplanar distance (d) of 0.44 nm calculated using the Bragg's equation: $n\lambda = 2d\sin\theta$; where, n, λ, and θ represents diffraction order, the wavelength of the x-ray source, and diffraction angle, respectively [28,29]. The mean crystallite size was calculated as 2.1 nm which is supported by previous reports [16,27]. The native PHB expressed diffraction peaks at 2θ of 13.6° (0 2 0), 16.9° (1 1 0), 21.5° (1 0 1), 22.6° (1 1 1), 25.5° (1 2 1) and at 27.1° (0 4 0) [30–32]. The peaks at 2θ of 13.6° (0 2 0) and 16.9° (1 1 0) indicated the orthorhombic unit cell and those at 2θ of 21° (1 0 1) and 22° (1 1 1) corresponded to α-PHB crystal whereas at 2θ of 25° (1 2 1) and 27° (0 4 0) indicated the PHB's semi-crystalline nature [31].

The XRD data confirmed the monoclinic system of CuO NPs, and well-matched the respective JCPDS card data (80-0076). The CuO NPs diffraction peaks appeared at 2θ of 32.60, 35.56, 38.77, and 48.89° with the respective diffraction planes of (1 1 0), (0 0 2), (1 1 1), and (-2 0 2) (with point group: 2/m and space group: C2/c) [27,33]. The average crystallite size (D) of CuO NPs was calculated as 50 nm using Debye-Scherrer's formula: $D = \frac{k\lambda}{\beta\cos\theta}$; where, k is an empirical constant (= 0.9 for the spherical particles), λ is x-ray wavelength (1.54 Å for CuKα), β is the full width at half maximum (FWHM), and θ is the diffraction angle [34]. The cell parameters were evaluated to be: a = 0.46891 nm, b = 0.34214 nm, and c = 0.51276 nm in agreement with the JCPDS card data (80-0076) [33].

The nanobiocomposite film expressed the characteristic diffraction peaks of the aforementioned precursors at 2θ of 19.9° (1 0 1), 13.6° (0 2 0), 16.9° (1 1 0), 21.5° (1 0 1), 22.6° (1 1 1), 25.5° (1 2 1), 27.1° (0 4 0), 32.60° (1 10), 35.56° (0 0 2), 38.77° (1 1 1), and 48.89° (−2 0 2). This indicated phase purity and successful formation of nanobiocomposite film. The sharp peaks associated with CuO NPs were tracked in the nanobiocomposite indicating their good dispersity in the matrix in the presence of PVA as binder and stabilizer [27]. The semi-crystalline

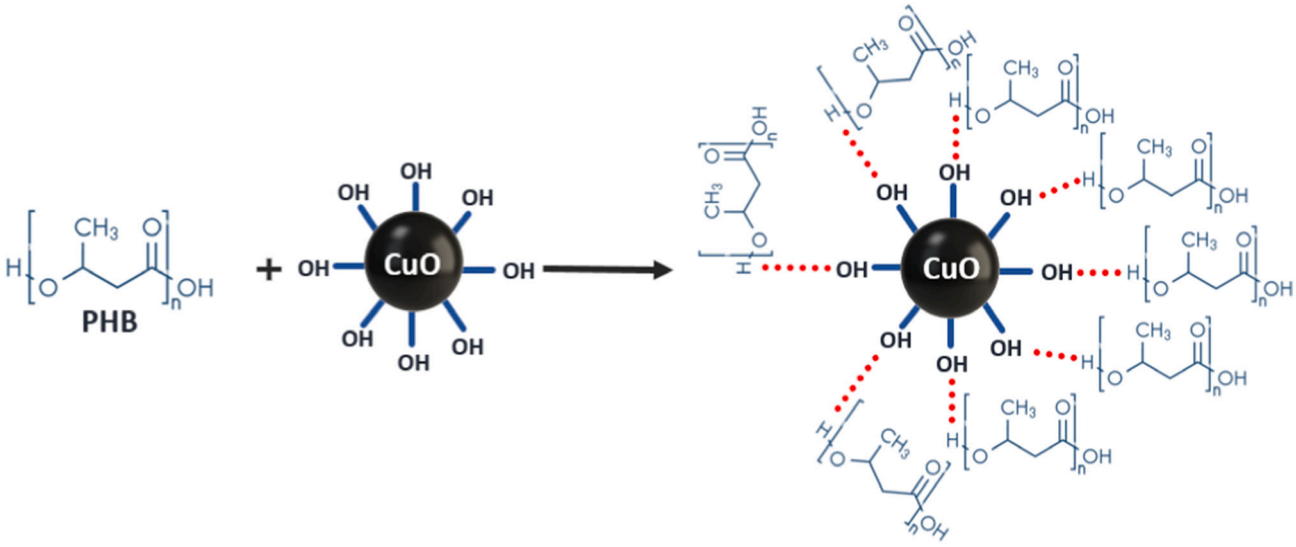

Fig. 2. Schematic illustration interaction of various components during PHB-based nanobiocomposite formation.

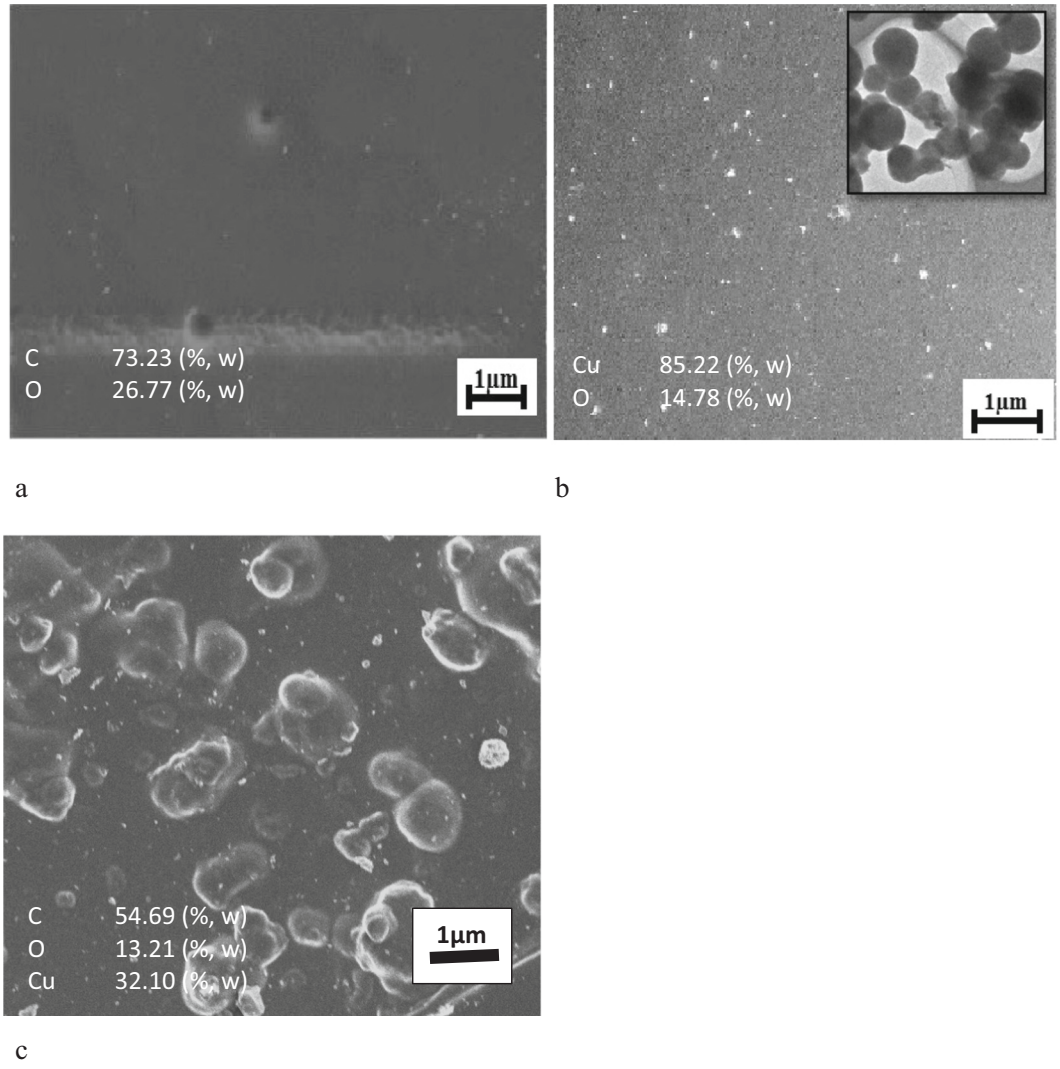

Fig. 3. SEM images of (a) PHB/PVA film, (b) CuO NPs, and (c) PHB/PVA/CuO nanobiocomposite.

nature of the synthesized nanobiocomposite was confirmed by the appearance of several crystalline peaks in its XRD spectrum. The FWHM of nanobiocomposite diffraction peaks indicates the possession of CuO NP's crystal structure even after their incorporation in the blended matrix. An overall reduction in the peak intensities associated with the PHB segments in the nanobiocomposite could be due to its reduced contents here as compared to that in the pristine PHB matrix.

3.5. Contact angle analysis

The investigation of the surface behavior of the synthesized films was done by taking contact angle measurements in a controlled chamber (at 25 °C) (Fig. 5A). Since PVA contains abundant -OH groups on its backbone so it exhibits inherent hydrophilicity – i.e., WCA being 57.45°. On incorporating PHB, the WCA of the blended composite appeared to be 74.50°, which could be attributed to the amphiphilic nature of PHB – containing both polar ester (-COOR) and nonpolar hydrocarbon moieties [13]. This amphiphilicity allows the PHB to engage in multiple non-covalent interactions with the PVA matrix may be in the form of dispersive forces which allow the PHB to transform the PVA's hydrophilic surface to hydrophobic [13]. On mediating CuO NPs in the biocomposite, the WCA was observed to be 88.86° (Fig. 5Ac) which could be ascribed to reduced hydrophilicity of nanobiocomposite surfaces due to the engagement with limited hydroxyl moieties on the CuO NPs surface. The CuO NPs could reduce the mobility of polymer chains in the blended composite by cross-linking its congeners and reducing the free spaces across the matrix, which in turn leads to increased hydrophobicity. This phenomenon could further be boosted due to enhanced surface roughness of the resultant films as supported by SEM analysis. The enhanced surface roughness limits the interaction and penetration of the wetting liquid to the nanobiocomposite surface [35]. The contact angle kinetics has been shown in Fig. 5B. The results depict that after 60 min of equilibration, the WCA on the native PVA film appeared to be 10°, on PHB/PVA film as 30° whereas on the nanobiocomposite film it expressed as 80°; indicating the aqueous stability of the resultant CuO incorporated composite. Eq. (3) was plotted to calculate the polar and dispersive components of solid surface energies (Fig. 5C) using diverse liquids of *n*-hexane, *n*-hexadecane, toluene, ethylene glycol and distilled water. The average surface energies of the native PVA, PHB/PVA and PHB/PVA/CuO NPs films turned out to be 41.26, 68.28 and 20.88 mJ/m^2. The results demonstrated that on mediating the CuO NPs in the PHB/PVA blend composite, the surface energy values decreased whereas the respective WCA values increased. This indicated that the incorporation of nanofiller made the nanobiocomposite film more stable thus lessening its need to adhere the aqueous media as with distilled water it expressed the contact angle of 88.86° whereas *n*-hexane approached to 0.5°.

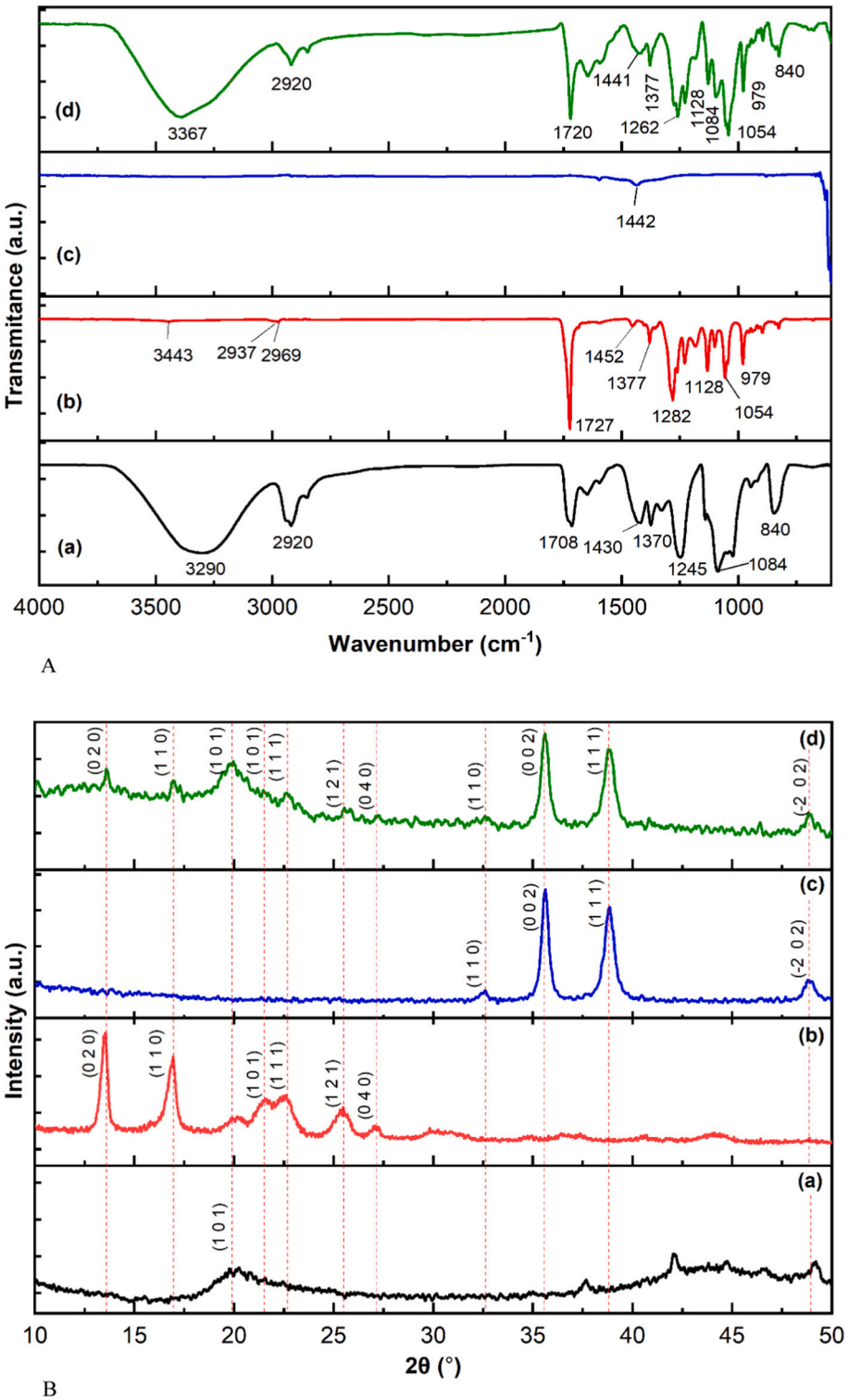

Fig. 4. A) FTIR spectra, and B) XRD patterns of (a) PVA, (b) PHB, (c) CuO NPs, and (d) PHB/PVA/CuO nanobiocomposite.

3.6. Mechanical analysis

The tensile strength and percentage elongation of the test samples are depicted in Fig. 5D. The results demonstrated that the native PVA film (of thickness 0.24 ± 0.02 mm) expressed the lowest tensile strength of 44.67 ± 3.20 N whereas PHB/PVA blended film (of thickness 0.25 ± 0.02 mm) showed an improved tensile strength of 66.43 ± 3.50 N which further improved to 86.24 ± 4.10 N in the case of nanobiocomposite film (of thickness 0.25 ± 0.02 mm); this was attributed to the reinforcement effect of the CuO NPs. The native PVA films established an H-bonding with the PHB congeners which resulted in improved tensile strength, further strengthened by incorporating CuO NPs in the PHB matrix [36,37]. A similar trend was observed in the case of percentage elongation. The native PVA film showed the elongation at the beak as 22.18 ± 1.10 (%) which improved to 36.70 ± 1.12 (%) and then to 35.36 ± 1.70 (%) in the case of PHB/PVA and nanobiocomposite, respectively. The inclusion of small side chains, such as methyl and ethyl groups, of PHB in the PVA resulted in higher tensile strength, and lower

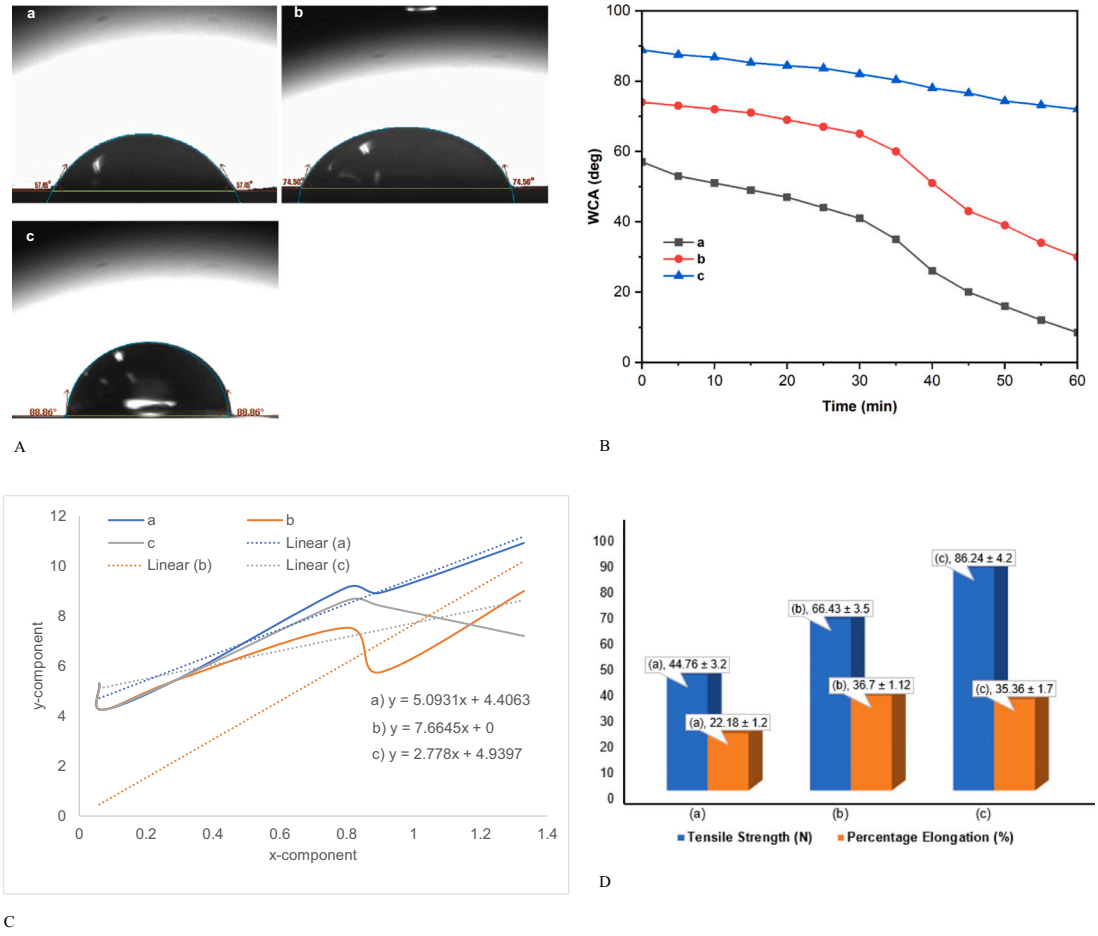

Fig. 5. A) Water contact angles, B) water contract angle kinetics, C) surface energy plots based on data obtained from Eq. (3) with diverse liquids, and D) tensile strength and percent elongation of a) PVA, b) PHB/PVA, and c) PHB/PVA/CuO films.

percentage elongation [38]. The incorporation of CuO NPs in the blended composite resulted in a significant increase in the tensile strength of the film which could be attributed to the uniform dispersion and intercalation of nanofiller within the polymer template [39,40].

3.7. Optical analysis

The UV–vis. absorption spectra of the test film samples are shown in Fig. 6A. On incorporating CuO NPs in the composite film, the absorbance curve red-shifted from 225 to 240 nm range to 210–240 nm which could be attributed to the H-bonding between the -OH groups of CuO and PHB/PVA matrix [27]. The absorption coefficients of the test film samples were calculated using Lambert Beer's law: $\alpha = 2.303\ \frac{A}{d}$; where, A is optical absorbance, α is the absorption coefficient and d is film thickness [27]. The $(\alpha h\nu)^{1/2}$ vs. $(h\nu)$ plot was evaluated for the determination of the absorption edge of the test samples (Fig. 6B). The absorption edge for PHB/PVA and the nanobiocomposite film was recorded to be 4.48 and 4.13 eV, respectively. The band gaps of the test films were calculated from the absorption edge data. The relation between α and hν was obtained by Tauc, Mott, and Devi's equation (for $\alpha > 10^4\ cm^{-1}$ and $h\nu < E_g$): $\alpha h\nu = D(h\nu - Eg)^{\gamma}$; where, D is the tail constant, E_g represents the optical band gap energy and γ is the exponent having the value of ½ for allowed indirect bandgap transition and 2 for the allowed direct bandgap transition [34]. The plot of $(\alpha h\nu)^{1/2}$ vs. $h\nu$ expressed the indirect bandgap energy (Fig. 6B). The $(\alpha h\nu)^{1/2}$ vs. $h\nu$ curve plot was evaluated for the indirect bandgap energy. The indirect bandgap for PHB/PVA was calculated to be 4.48 eV. Upon incorporation of CuO NPs in the PHB/PVA matrix, the indirect bandgap reduced to 4.13 eV. The $(\alpha h\nu)^2$ vs. $h\nu$ plot was interpreted for the calculation of the direct bandgap energy shown in Fig. 6C. The $(\alpha h\nu)^2$ vs. $h\nu$ plot was evaluated for the direct bandgap energy of 5.15 eV was calculated for PHB/PVA which was reduced to 4.71 eV for the resultant nanobiocomposite.

3.8. AC conductivity

Fig. 6D shows the effect of the CuO NPs insertion and AC conductivity (σ_{ac}) on the prepared samples. The σ_{ac} conductivity was calculated using Eq. $\sigma_{ac} = 2\pi f\ \varepsilon_o\varepsilon''$; where, f, ε_o, and ε'' are frequency, vacuum permittivity, and loss components of the permittivity, respectively [41]. The relationship between σ_{ac} and applied frequency was observed to be directly proportional up to 8 MHz which might be attributed to an enhanced oscillation of electronic species across the nanobiocomposite. At still higher frequency, the σ_{ac} deceased as the electrons/holes oscillate so fast that the net charge movement along the particular direction becomes smaller as compared to that in the presence of a low-frequency field [17,41]. The σ_{ac} values of the prepared PHB/PVA and CuO NPs mediated biocomposite films were observed as 0.051 and 0.060 S/cm, respectively, at 8 MHz. The increased σ_{ac} in the latter case could be attributed to enhanced charge carriers and their mobility induced by the CuO NPs insertion - being an n-type semiconductor [17].

3.9. Cyclic voltammetry

The CVs of PHB, CuO, and PHB/CuO deposited GCE at the scan rates of 10, 50, and 100 mV s^{-1} against 5 mM KFeCN in the 1 M KCl media are

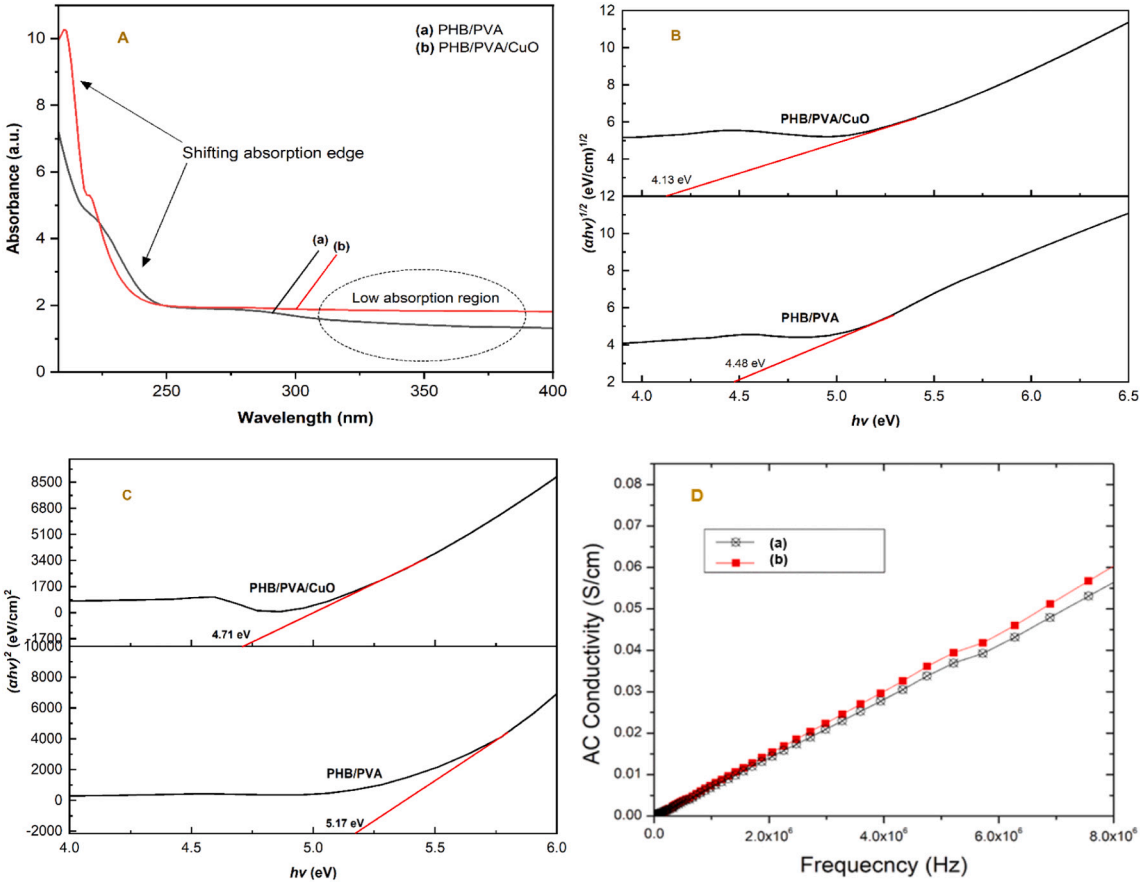

Fig. 6. A) Absorbance spectra, B) $(\alpha h\nu)^{1/2}$ vs. (hν), C) $(\alpha h\nu)^2$ vs ($h\nu$), and D) AC conductivity for PHB/PVA and PHB/PVA/CuO films.

shown in Fig. 7. An oxidation peak current of 18.64 μA was observed at 0.28 *V* (Fig. 7a) for the PHB deposited on the GCE. On incorporating CuO NPs in the PHB matrix, the oxidation peak current shifted to 24.68 μA at the respective peak potential of 0.29 V (Fig. 7c). This increase in the peak current could be attributed to enhanced electrocatalytic activity induced by CuO NPs in the nanobiocomposite [42,43]. The enhanced electrochemical performance of the resultant nanobiocomposite deposit could be ascribed to the enhanced surface area provided by the CuO NPs offering increased binding sites for the analyte [42,44].

The effect of scan rate was studied by performing CV analyses for all prepared samples at different scan rates i.e., 10, 50, and 100 m*V* s^{-1} as depicted in Fig. 7 with the key electrochemical parameters in Table 1. The increased cathodic current with the scan rate has been reported for CuO NPs deposited on GCE in the determination of uric acid [43,44]. The peak-to-peak potential separation (ΔE) for the PHB deposit on GCE was recorded as 0.13 V which gradually lowered to 0.10 V for PHB/CuO nanobiocomposite. The decrease in ΔE on incorporating the CuO NPs in the PHB-based sensor indicated enhanced sensor kinetics and good reversibility of the electrochemical surfaces which ensured their electrochemical potential. The CVs have been drawn for the AA (10 mM) at the scan rate of 100 mV s^{-1} against bare and PHB/CuO modified GCEs at different CuO NP concentrations (Fig. 7d). The background medium used in the CV analysis was 50 mM PBS. The CV response of bare GCE showed insignificant redox peaks (Fig. 7d); whereas, the PHB/CuO-coated electrode with 3 % (*w*/w) CuO NPs yielded the highest oxidation peak current of 36.35 ± 0.20 μA at the respective peak potential of 0.21 V (Fig. 7d).

3.10. Sensor analytics

The CV scans were also recorded against different concentrations of AA i.e., 0.2–10.0 mM (Fig. 7e), and the respective outcomes have been presented in Table 2. It was recorded that the peak currents increased gradually from 5.58 to 36.25 μA with increasing the AA concentration from 0.2 to 10.0 mM, respectively (with the linear regression $r = 0.996$) (Fig. 7f). The limit of detection (LoD) and limit of quantification (LoQ) for the PHB/CuO sensor were observed as 1.51 and 4.48 mM, respectively, against the AA. This indicates the applicability of the prepared biosensing for diagnostics [43]. This indicates the electrocatalytic potential of the fabricated nanobiocomposite deposited GCE surface.

3.11. Biosensor stability

Fig. 7g expresses the stability and efficiency of the modified electrode surfaces tracked for up to three months. As has been stated above that the PHB is a biodegradable polymer that is vulnerable to bacterial degradation. The CuO NPs, on the other hand, are antibacterial thus their incorporation in the PHB matrix might retard its undesirable biodegradation under ambient conditions without packing it. The results demonstrated their appropriate stability for up to three months at least which could further be improved on proper packing, shelving, and preserving of the test electrodes. The test electrodes expressed about 99 % reproducibility after the mentioned time spawn.

4. Conclusions

The biocompatible PHB-based nanocomposite was synthesized through the solution casting approach. The PHB was used as the base, CuO NPs as a reinforcer, and PVA as binder and stabilizer. The structural and morphological analyses expressed effective mediation of CuO NPs in the PHB/PVA matrix thereby confirming the successful formation and purity of the nanobiocomposite. The WCA measurement, mechanical,

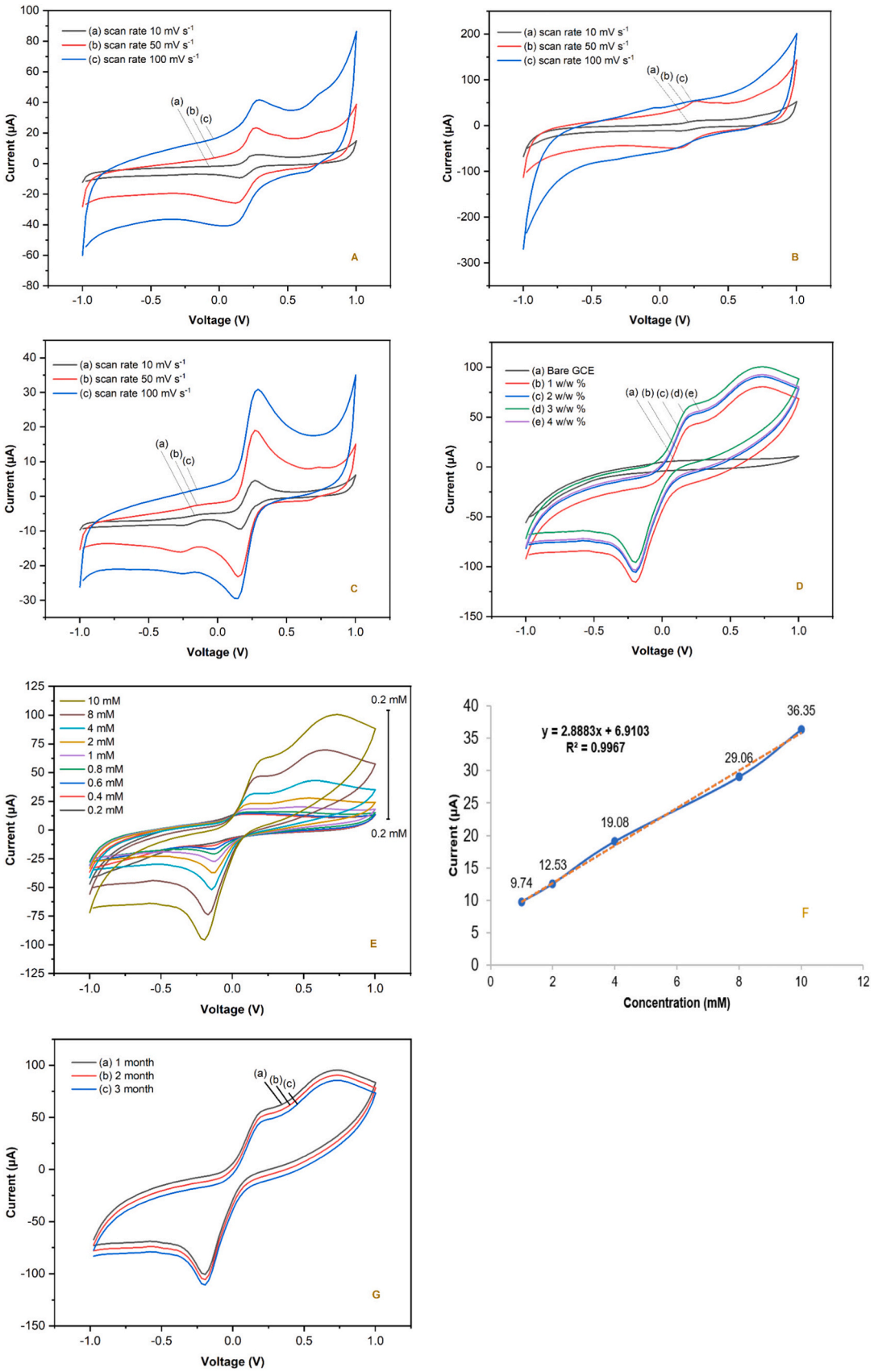

Fig. 7. Cyclic voltammograms of A) PHB, B) CuO NPs, and C) PHB/CuO nano bio-composite at a scan rate of 10, 50, and 100 mV s^{-1}; Cyclic voltammograms of D) CV response of Bare electrode and PHB/CuO modified electrode with different concentration of CuO NPs towards AA, and E) PHB/CuO modified electrode response towards 0.2–10 mM AA, at scan rate 100 mV s^{-1} in 50 mM PBS; F. Linear regression graph for PHB/CuO modified electrode against AA, $R^2 = 0.996$; G. Cyclic voltammograms of PHB/CuO sensor towards 10 mM of AA after a period 1–3 month.

Table 1
Effect of scan rate on the CV performance indicators.

Scan rate (mV s^{-1})	PHB					CuO NPs					PHB/CuO nanobiocomposite				
	Ip,a (μA)	Ip,c (μA)	Ep,a (V)	Ep,c (V)	ΔE (V)	Ip,a (μA)	Ip,c (μA)	Ep,a (V)	Ep,c (V)	ΔE (V)	Ip,a (μA)	Ip,c (μA)	Ep,a (V)	Ep,c (V)	ΔE (V)
10	4.91	11.39	0.27	0.14	0.13	7.79	6.93	0.31	0.15	0.16	0.32	8.26	0.26	0.16	0.10
50	15.48	17.09	0.26	0.11	0.15	20.91	27.38	0.26	0.12	0.14	18.31	20.18	0.27	0.15	0.12
100	18.64	23.07	0.28	0.03	0.25	–	–	–	–	–	24.68	25.42	0.29	0.13	0.16

Table 2
Effect of various concentrations of analyte on the CV performance indicators.

Concentration (mM)	Ip,a (μA)	Ip,c (μA)	Ep,a (V)	Ep,c (V)	ΔE (V)
0.2	5.58	1.46	0.07	−0.16	0.23
0.4	5.75	3.44	0.07	−0.16	0.23
0.6	6.20	6.17	0.09	−0.14	0.23
0.8	7.09	10.98	0.09	−0.12	0.21
1.0	9.74	17.43	0.10	−0.11	0.21
2.0	12.53	25.37	0.12	−0.12	0.24
4.0	19.08	37.81	0.14	−0.14	0.28
8.0	29.06	52.33	0.17	−0.17	0.34
10.0	36.35	63.86	0.21	−0.19	0.40

and optical analysis suggested decreased hydrophilicity, improved ultimate tensile strength, and a low bandgap of the resultant nanobiocomposite thereby enhancing its potential for optoelectronic devices. The electrochemical potential of the prepared nanobiocomposite was exploited by the successful detection of the KFeCN and ascorbic acid as model analytes under cyclic voltammetry. Based on the research outcomes, so for, it could be proposed that the CuO NPs mediated nanocomposite films could find potential applications in the fabrication of electromagnetic devices and intelligent materials. A controlled mediation of CuO as nanofiller in the PHB-based nanobiocomposite could offer eco-friendly and renewable articles with comparable physicomechanical and electrical attributes. In future studies, some piezoelectric congeners may also be included in the PHB-based nanobicomposites to extend their properties and usability in a wide range of electrical and electronic applications.

Declaration of competing interest

The authors declare neither present nor potential conflict of interest with the study reported here.

Acknowledgment

The authors acknowledge the financial support (as NRPU-9566) from the Higher Education Commission, Pakistan for the completion of this study.

References

[1] D. Rohilla, S. Chaudhary, A. Umar, An overview of advanced nanomaterials for sensor applications, Eng. Sci. 16 (2021) 47–70, https://doi.org/10.30919/es8d552.
[2] M.N. Padvi, A.V. Moholkar, S.R. Prasad, N.R. Prasad, A critical review on design and development of gas sensing materials, Eng. Sci. 15 (2021) 20–37, https://doi.org/10.30919/es8d431.
[3] S. Mishra, P. Chaudhary, B.C. Yadav, A. Umar, P. Lohia, D.K. Dwivedi, Fabrication and characterization of an ultrasensitive humidity sensor based on chalcogenide glassy alloy thin films, Eng. Sci. 15 (2021) 138–147, https://doi.org/10.30919/es8d500.
[4] A. Arun, P. Malrautu, A. Laha, S. Ramakrishna, Gelatin nanofibers in drug delivery systems and tissue engineering, Eng. Sci. 16 (2021) 71–81, https://doi.org/10.30919/es8d527.
[5] Y. Wu, J. Liu, S. Lin, K. Huang, E. Chen, K. Huang, M. Lei, New pressure matrix array sensor composed of flexible mechanical sensor elements, Eng.Sci. (2022), https://doi.org/10.30919/es8d626.
[6] X. Chang, L. Chen, J. Chen, Y. Zhu, Z. Guo, Advances in transparent and stretchable strain sensors, Adv. Compos. Hybrid Mater. 4 (2021) 435–450, https://doi.org/10.1007/s42114-021-00292-3.
[7] K.R. Srivastava, S. Awasthi, P.K. Mishra, P.K. Srivastava, Biosensors/molecular tools for detection of waterborne pathogens, in: M.N.V. Prasad, A. Grobelak (Eds.), Waterborne Pathogens, Butterworth-Heinemann, 2020, pp. 237–277, https://doi.org/10.1016/B978-0-12-818783-8.00013-X.
[8] Z.A. Raza, S. Munim, A. Ayub, Recent developments in polysaccharide-based electrospun nanofibers for environmental applications, Carbohyd. Res. 510 (2021), 108443, https://doi.org/10.1016/j.carres.2021.108443.
[9] N. Jiang, D. Hu, Y. Xu, J. Chen, X. Chang, Y. Zhu, Y. Li, Z. Guo, Ionic liquid enabled flexible transparent polydimethylsiloxane sensors for both strain and temperature sensing, Adv. Compos. Hybrid Mater. 4 (2021) 574–583, https://doi.org/10.1007/s42114-021-00262-9.
[10] S.S. Silva, L.C. Rodrigues, E.M. Fernandes, R.L. Reis, Fundamentals on biopolymers and global demand, in: M.A. de Moraes, C.F. da Silva, R.S. Vieira (Eds.), Biopolymer Membranes And Films, Elsevier, 2020, pp. 3–34, https://doi.org/10.1016/B978-0-12-818134-8.00001-8.
[11] M. Culebras, G.A. Collins, A. Beaucamp, H. Geaney, M.N. Collins, Lignin/Si hybrid carbon nanofibers towards highly efficient sustainable Li-ion anode materials, Eng. Sci. 17 (2022) 95–203, https://doi.org/10.30919/es8d608.
[12] Y. Zhao, X. Xia, J. Zhou, Z. Huang, F. Lei, X. Tan, D. Yu, Y. Zhu, H. Xu, Thermoresponsive behavior of non-isocyanate poly(hydroxyl)urethane for biomedical composite materials, Adv. Compos. Hybrid Mater. (2021), https://doi.org/10.1007/s42114-021-00379-x.
[13] B. McAdam, M.B. Fournet, P. McDonald, M. Mojicevic, Production of polyhydroxybutyrate (PHB) and factors impacting its chemical and mechanical characteristics, Polymers 12 (2020) 2908, https://doi.org/10.3390/polym12122908.
[14] M. Shabbir, Z.A. Raza, T.H. Shah, M.R. Tariq, Recent progress in graphenes: synthesis, covalent functionalization and environmental applications, J. Nanostruct. Chem. (2022), https://doi.org/10.1007/s40097-021-00467-w.
[15] S. Riaz, Z.A. Raza, M.I. Majeed, Preparation of cadmium sulfide nanoparticles and mediation thereof across poly(hydroxybutyrate) nanocomposite, Polym. Bull. 77 (2020) 775–791, https://doi.org/10.1007/s00289-019-02775-2.
[16] M. Aslam, Z.A. Raza, A. Siddique, Fabrication and chemo-physical characterization of CuO/chitosan nanocomposite-mediated tricomponent PVA films, Polym. Bull. 78 (2021) 1955–1965, https://doi.org/10.1007/s00289-020-03194-4.
[17] M. Aslam, M.A. Kalyar, Z.A. Raza, Effect of separate zinc, copper and graphene oxides nanofillers on electrical properties of PVA based composite strips, J. Electron. Mater. 48 (2019) 1116–1121, https://doi.org/10.1007/s11664-018-6793-5.
[18] P. Malik, R. Gupta, V. Malik, R.K. Ameta, Emerging nanomaterials for improved biosensing, Meas. Sensors 16 (2021), 100050, https://doi.org/10.1016/j.measen.2021.100050.
[19] A. Fatima, S. Yasir, M. Ul-Islam, T. Kamal, Md.W. Ahmad, Y. Abbas, S. Manan, M. W. Ullah, G. Yang, Ex situ development and characterization of green antibacterial bacterial cellulose-based composites for potential biomedical applications, Adv. Compos. Hybrid. Mater. 5 (2022) 307–321, https://doi.org/10.1007/s42114-021-00369-z.
[20] Y. Lu, C. Li, Y. Wu, Preparation of dimer acid-based polyamide film by solution casting method and its properties optimization, J. Polym. Res. 28 (2021) 68, https://doi.org/10.1007/s10965-021-02441-0.
[21] A.S. Alshammari, Carbon-based polymer nanocomposites for sensing applications, in: A.F. Ismail, P.S. Goh (Eds.), Carbon-based Polymer Nanocomposites for Environmental And Energy Applications, Elsevier, 2018, pp. 331–360, https://doi.org/10.1016/B978-0-12-813574-7.00014-9.
[22] E. Hernández-Núñez, C.A. Martínez-Gutiérrez, A. López-Cortés, Ma.L. Aguirre-Macedo, C. Tabasco-Novelo, M.O. González-Díaz, J.Q. García-Maldonado, Physicochemical characterization of poly(3-hydroxybutyrate) produced by Halomonas salina, isolated from a hypersaline microbial mat, J. Polym. Environ. 27 (2019) 1105–1111, https://doi.org/10.1007/s10924-019-01417-y.
[23] H. Hendrawan, F. Khoerunnisa, Y. Sonjaya, A.D. Putri, Poly(vinyl alcohol)/glutaraldehyde/Premna oblongifolia merr extract hydrogel for controlled-release and water absorption application, IOP Conf. Ser.: Mater. Sci. Eng. 509 (2019), 012048, https://doi.org/10.1088/1757-899X/509/1/012048.
[24] M.F.H. Al-Kadhemy, S.A. Ibrahim, J.A.S. Salman, Studying the physical properties polyvinyl alcohol polymer mixture with silica nanoparticles and its application as pathogenic bacteria inhibitor, AIP Conf. Proc. 2290 (2020), 050013, https://doi.org/10.1063/5.0028817.
[25] C. Trakunjae, A. Boondaeng, W. Apiwatanapiwat, W.A. Kosugi, T. Arai, K. Sudesh, P. Vaithanomsat, Enhanced polyhydroxybutyrate (PHB) production by newly isolated rare actinomycetes Rhodococcus sp. strain BSRT1-1 using response surface

methodology, Sci. Rep. 11 (2021) 1896, https://doi.org/10.1038/s41598-021-81386-2.
[26] M. Elango, M. Deepa, R. Subramanian, A.M. Musthafa, Synthesis, characterization, and antibacterial activity of polyindole/Ag-CuO nanocomposites by reflux condensation method, Polym. Plast. Technol. Eng. 57 (2018) 1440–1451, https://doi.org/10.1080/03602559.2017.1410832.
[27] M. Aslam, M.A. Kalyar, Z.A. Raza, Fabrication of nano-CuO-loaded PVA composite films with enhanced optomechanical properties, Polym. Bull. 78 (2021) 1551–1571, https://doi.org/10.1007/s00289-020-03173-9.
[28] A. Ali, Y.W. Chiang, R.M. Santos, X-ray diffraction techniques for mineral characterization: a review for engineers of the fundamentals, applications, and research directions, Minerals 12 (2022) 205, https://doi.org/10.3390/min12020205.
[29] X. Zhang, K. Tang, X. Zheng, Electrospinning and crosslinking of COL/PVA nanofiber-microsphere containing salicylic acid for drug delivery, J. Bionic Eng. 13 (2016) 143–149, https://doi.org/10.1016/S1672-6529(14)60168-2.
[30] J.P. Florez, M. Fazeli, A.A. Simão, Preparation and characterization of thermoplastic starch composite reinforced by plasma-treated poly (hydroxybutyrate) PHB, Int. J. Biol. Macromol. 123 (2019) 609–621, https://doi.org/10.1016/j.ijbiomac.2018.11.070.
[31] S. Pradhan, P.K. Dikshit, V.S. Moholkar, Production, ultrasonic extraction, and characterization of poly (3-hydroxybutyrate) (PHB) using Bacillus megaterium and Cupriavidus necator, Polym. Adv. Technol. 29 (2018) 2392–2400, https://doi.org/10.1002/pat.4351.
[32] S. Riaz, Z.A. Raza, M.I. Majeed, T. Jan, Synthesis of zinc sulfide nanoparticles and their incorporation into poly (hydroxybutyrate) matrix in the formation of a novel nanocomposite, Mater. Res. Express 5 (2018), 055027, https://doi.org/10.1088/2053-1591/aac1f9.
[33] U. Halder, R.K. Roy, R. Biswas, D. Khan, K. Mazumder, R. Bandopadhyay, Synthesis of copper oxide nanoparticles using capsular polymeric substances produced by Bacillus altitudinis and investigation of its efficacy to kill pathogenic Pseudomonas aeruginosa, Chem. Eng. J. Adv. 11 (2022), 100294, https://doi.org/10.1016/j.ceja.2022.100294.
[34] M. Awale, L. Kathwate, S. Lokhande, Synthsis, structural and optical properties of Zn 1-X Co X O of thin films by spray pyrolysis method, Mater. Sci. 11 (2019) 6–10, https://doi.org/10.9790/4861-1103020610.
[35] S.M. Hasheminya, R.R. Mokarram, B. Ghanbarzadeh, H. Hamishekar, H.S. Kafil, Physicochemical, mechanical, optical, microstructural and antimicrobial properties of novel kefiran-carboxymethyl cellulose biocomposite films as influenced by copper oxide nanoparticles (CuONPs), Food Packag. ShelfLife 17 (2018) 196–204, https://doi.org/10.1016/j.fpsl.2018.07.003.
[36] O. Olejnik, A. Masek, J. Zawadziłło, Processability and mechanical properties of thermoplastic polylactide/polyhydroxybutyrate (PLA/PHB) bioblends, Materials (Basel) 14 (2021) 898, https://doi.org/10.3390/ma14040898.
[37] W. Zou, J. Huang, J. Su, W. Zeng, Y. Liang, R. Chen, H. Zhang, Y. Min, Z. Guo, Review on modification of poly(lactic acid) in physical and mechanical properties, Eng. Sci. 6 (2021) 3–11, https://doi.org/10.30919/esfaf562.
[38] J. Yu, Microbial production of bioplastics from renewable resources, in: S.T. Yang (Ed.), Bioprocessing for Value-added Products From Renewable Resources, Elsevier, 2007, pp. 585–610, https://doi.org/10.1016/B978-044452114-9/50024-4.
[39] M. Aslam, M.A. Kalyar, Z.A. Raza, Investigation of zinc oxide-loaded poly(vinyl alcohol) nanocomposite films in tailoring their structural, optical and mechanical properties, J. Electron. Mater. 47 (2018) 3912–3926, https://doi.org/10.1007/s11664-018-6270-1.
[40] Z. Yu, Z. Yan, F. Zhang, J. Wang, Q. Shao, V. Murugadoss, A. Alhadhrami, G.A. M. Mersal, M.M. Ibrahim, Z.M. El-Bahy, Y. Li, M. Huang, Z. Guo, Waterborne acrylic resin co-modified by itaconic acid and γ-methacryloxypropyl triisopropoxidesilane for improved mechanical properties, thermal stability, and corrosion resistance, Prog. Org. Coat. 168 (2022), 106875, https://doi.org/10.1016/j.porgcoat.2022.106875.
[41] A.M. El-hadi, A.M. Abd-Elbary, S.M. Alluqmani, The role of polyaniline and plasticizer on the development of the electrical conductivity of PHB composites, J. Compos. Mater. 53 (2019) 2305–2314, https://doi.org/10.1177/0021998319826348.
[42] B. Tehseen, A. Rehman, M. Rahmat, H.N. Bhatti, A. Wu, F.K. Butt, G. Naz, W. S. Khan, S.Z. Bajwa, Solution growth of 3D MnO2 mesh comprising 1D nanofibres as a novel sensor for selective and sensitive detection of biomolecules, Biosens. Bioelectron. 117 (2018) 852–859, https://doi.org/10.1016/j.bios.2018.06.061.
[43] R. Shashanka, B.E.K. Swamy, Simultaneous electro-generation and electro-deposition of copper oxide nanoparticles on glassy carbon electrode and its sensor application, SN Appl. Sci. 2 (2020) 956, https://doi.org/10.1007/s42452-020-2785-1.
[44] J.A. Buledi, S. Ameen, S.A. Memon, A. Fatima, A.R. Solangi, A. Mallah, F. Karimi, S. Malakmohammadi, S. Agarwal, V.K. Gupta, An improved non-enzymatic electrochemical sensor amplified with CuO nanostructures for sensitive determination of uric acid, Open Chem. 19 (2021) 481–491, https://doi.org/10.1515/chem-2021-0029.